Engineering Science and Technology, an International Journal 24 (2021) 890–898

HOSTED BY

Contents lists available at ScienceDirect

Engineering Science and Technology, an International Journal

journal homepage: www.elsevier.com/locate/jestch

Full Length Article

Experimental evaluation of water cycle technique for control parameters optimization of double-fed induction generator-based wind turbine

Hale Bakir [a,*], Adel Merabet [b], Rupak Kanti Dhar [b], Ahmet Afsin Kulaksiz [a]

[a] Department of Electrical and Electronics Engineering, Konya Technical University, Konya, Turkey
[b] Division of Engineering, Saint Mary's University, Halifax, NS B3H 3C3, Canada

ARTICLE INFO

Article history:
Received 5 September 2020
Revised 9 December 2020
Accepted 26 December 2020
Available online 25 January 2021

Keywords:
Doubly-fed induction generator
Vector control
Water cycle
Optimization

ABSTRACT

In this paper, a nature-inspired optimization algorithm is employed for parametric tuning of proportional-integral controllers in the vector control of a grid-linked doubly-fed induction generator energy system. The optimization approach is based on the nature-inspired computing technique from the water cycle. The vector control system includes loops for dc-link voltage control at the grid side converter and the rotor current at the rotor side converter. The water cycle optimization is implemented to tune six control parameters by minimizing a cost function carried out using the tracking errors. The cost function value, required in the optimization process, is carried out from a simulated grid-linked doubly-fed induction generator energy system. The optimized control parameters are tested on an experimental setup. Experimental results, obtained for a grid-linked doubly-fed induction generator energy system in terms of different optimization methods and conditions, are provided to demonstrate the effectiveness of water cycle optimization technique. As a result of the comparative analysis, it is observed that water cycle technique offers better results in minimizing the overshoot and the response time.

1. Introduction

Recently, environmental problems related to the increase in electricity consumption, exhaustion of fossil fuels and the use of non-renewable resources have encouraged the use of renewable resources. Wind is one of the most promising distributed energy resources to meet the electricity demand and the share of wind power generation is increasing worldwide [1]. A grid-linked doubly-fed induction generator (DFIG) energy system, equipped with wind turbine (WT), has been deployed for high energy generation. This wind energy configuration has been investigated in several studies. This is due to its advantages in decoupled active-reactive power control, high converter efficiency and low cost, and reduced mechanical stress. Furthermore, the DFIG system can operate under wide range of wind speeds and the energy capture can be enhanced compared to variable speed turbine using a cage bar induction machine. However, controlling of DFIG is harder than controlling other machines, and it is vital to observe the generator behavior in fault conditions or normal operation by power converters and controllers [2].

In the DFIG system, a back-to-back converter structure is used for the power feeding and transfer. This configuration comprises separate rotor side converter (RSC) and grid side converter (GSC). At the GSC, the dc-link is regulated to have a constant voltage for proper power transfer. Furthermore, the GSC can be controlled to compensate or remove the reactive power for unstable conditions [3]. At the RSC, the required magnetization currents, in rotor windings, can be governed to regulate the active and reactive powers at the DFIG stator [4].

Adjustment methods for DFIG energy systems are considered as an important issue in the presence of high amplitude disorders. In most applications, control systems have employed proportional-integral (PI) controllers based vector control scheme to regulate the dc-link voltage, rotor currents, or active-reactive power. According to the reported studies, setting the PI controller parameters does not provide a satisfactory result with the basic adjustment methods. Furthermore, the minimization of the performance indices is confronted with indeterminate dynamics, time delays and nonlinearities. The cyclical and slow recovery of incorrectly setting of PI parameters, poor stability and worst-case scenario may cause the system operation to crash. These outputs provide large oscillations and higher settling time in high power systems. Therefore, it is required to automatically set the PI control

* Corresponding author at: Department of Electrical and Electronics Engineering, Faculty of Engineering and Natural Sciences, Konya Technical University, 42250 Konya, Turkey.
E-mail addresses: hbakir@ktun.edu.tr (H. Bakir), adel.merabet@smu.ca (A. Merabet), rupak0013@lus.ac.bd (R.K. Dhar), aakulaksiz@ktun.edu.tr (A.A. Kulaksiz).
Peer review under responsibility of Karabuk University.

https://doi.org/10.1016/j.jestch.2020.12.024
2215-0986/

parameters to provide better responses. In this field, researchers are conducting studies to find efficient methods to optimize the control parameters through artificial intelligence tools or nature-inspired algorithms. The present research is therefore intended to make contributions to the literatures on optimal design of the PI controllers, using Water Cycle Algorithm (WCA) technique for performance improvement of an experimental grid-linked DFIG energy system.

Many recent studies have been devoted to optimizing the control parameters in control circuit of various systems. Traditionally, the conventional Ziegler–Nichols method can be used to tune proportional-integral-derivative (PID) control parameters, as in [5], or Kharitonov/Nyquist optimization methods as proposed in [6]. A hybrid Taguchi-genetic algorithm (HTGA) was developed, in [7], to select the optimal values of the PID control parameters. In AC micro-grids, PI-based frequency control was investigated, where intelligent control synthesis was developed and compared to other PI control design techniques such as fuzzy PI and Ziegler-Nichols [8]. Heuristic search methods were studied for optimal design of the PI control parameters. In [9], genetic algorithms optimization (GAO) was used to tune the parameters of the PI controllers of the frequency converter of wind energy conversion system (WECS). A harmony search algorithm (HSA) was used in [10], for the optimal design of the PI controllers in the converter at the grid-side voltage source. These studies have achieved successful results in supporting the system voltage within the required level using advanced optimization techniques [11]. [12] used a fuzzy algorithm on multiple objective particle swarm optimization, genetic algorithm, bees, and reinforcement learning based on the frequency sensitivity margin of a water turbine governor to optimize the proportional gain and integral gain. The authors proposed the determination of grid frequency deviations and PI parameters for the hydro-turbine. Their algorithm focused on reducing the rise time and maintaining superior grid frequency deviation performance, and simulation results are used to verify the presented algorithm. For the optimization of numerical functions, many nature inspired algorithms have been developed [13–14]. [13] proposed a novel metaheuristic optimization algorithm called circular water waves (CWW). They tested CWW algorithm with eight different benchmark functions and used these functions to compare with artificial bee colony (ABC) and particle swarm optimization (PSO). Some parts of the study demand improvement such as better mechanism for randomized best points, decision mechanism for radius, and radius update mechanism. In another simulation study performed for wind turbine system [15] whale optimization algorithm (WOA) has been used for the effective tuning of the PI controllers. The study demonstrate that the WOA based controller can enhance power system stability for Type-2 wind turbines. One of the recent optimization methods, that was observed to be efficient and simple compared to other methods, is the WCA. This technique has shown good performances with respect to convergence, computation, and precision [16]. The WCA algorithm was proposed, in [17], to tune the parameters of the PID controllers and checked against random disturbances in different conditions. The power system as micro-grid, control circuit, converter operation can be further enhanced with the use of the WCA for optimal control design in the PI control scheme [18].

Examining the previous work, it can be observed that most of the studies are based on simulations and an experimental evaluation study on this field still needs more research. A recent study on this field was conducted by Hato et al. on the superiority of WCA-based PI Control over other methods [19]. Although significant merits of WCA-based algorithm is shown, the results of the study was limited on simulations. The optimal design of PI and PID controllers have also been employed recently for hybrid renewable energy applications. [20] proposed an efficient adaptive sine cosine algorithm to predict the optimal settings of the PID controllers in hybrid renewable energy system consisting of photovoltaic source, wind turbine and battery storage. The objective of the study was to decrease the fluctuations of the output voltage, current and power in a hybrid renewable energy system. The authors verified the system performance using simulation results for variations of the wind speed, solar irradiation, and temperature. In our study, a real-time measurement was made with OPAL-RT technology by establishing a direct experimental application system. The water cycle optimization is used for optimal design of the PI controllers in order to operate a grid-linked DFIG energy system. The system modeling is integrated in the optimization method to minimize the cost function based on the tracking errors, which is considered as one of the main contributions. The efficiency of the WCA based PI controller method has been proven by comparing it with the traditional PI controller and the genetic algorithm based PI controller. The results are also evaluated using different performance criteria to improve the optimization of the proposed system. The main contribution of this work is to eliminate the drawbacks of classical tuning methods by employing WCA algorithm for optimal design of PI controllers and improve the operation of vector control scheme of a DFIG-based wind energy system. Furthermore, in the WCA method, all the DFIG dynamics are presented in its implementation.

This paper is composed as follows: the grid-linked DFIG energy system, used in the optimization process for the cost function, is modelled in Section 2. The PI control-based vector control scheme is discussed for GSC and RSC, in Section 3. The WCA algorithm is detailed in Section 4, as design variables for PI control parameters. Section 5 gives and discusses the experimental results and analysis. Section 6 provides conclusion.

2. Grid-linked DFIG wind turbine

2.1. DFIG modeling

The DFIG energy system is linked to the grid via the back-to-back converters and the stator as shown in Fig. 1. The DFIG system

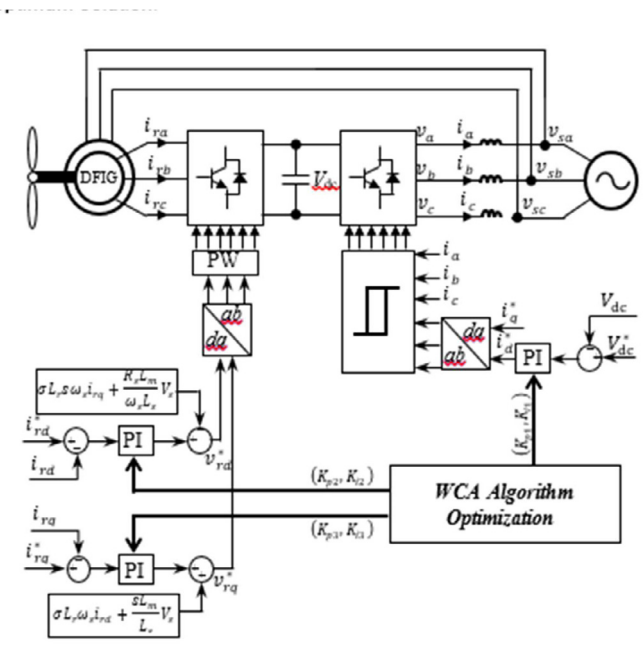

Fig. 1. Optimization, control and model for DFIG energy system.

includes a dynamometer, as a prime mover, a DFIG, AC-DC converter and DC-AC back-to-back converters, a resistive-inductive (*RL*) filter and voltage source to imitate the grid.

The AC-DC rotor side converter is operated to govern active-reactive power at the stator through controlling the rotor currents. The rotor current dynamics is modeled under the stator flux orientation in the synchronously rotating reference frame (*d-q*), (φ_{sd}=φ_s,φ_{sq} = 0) and the stator voltage alignment similar to [21,22].

$$\begin{cases} v_{sd} = 0 \\ v_{sq} = \omega_s \varphi_s = V_s \end{cases} \tag{1}$$

where, v_{sd} is the *d*-axis stator voltage and v_{sq} is the *q*-axis stator voltage, φ_{sd} is the *d*-axis stator flux, φ_{sq} is the *q*-axis stator flux, ω_s is the synchronous angular speed.

Then, the rotor current dynamics can be modelled by

$$\begin{cases} \frac{di_{rd}}{dt} = -ai_{rd} + s\omega_s i_{rq} + \frac{R_s b}{\omega_s} V_s + \frac{1}{\sigma L_r} v_{rd} \\ \frac{di_{rq}}{dt} = -ai_{rq} - s\omega_s i_{rd} - bsV_s + \frac{1}{\sigma L_r} v_{rq} \end{cases} \tag{2}$$

$\sigma = 1 - \frac{L_m^2}{L_s L_r}$, $s = \frac{\omega_s - \omega_r}{\omega_s}$, $a = \frac{R_r L_s^2 + R_s L_m^2}{\sigma L_s^2 L_r}$, $b = \frac{L_m}{\sigma L_s L_r}$ where, *s* is the slip, R_r is the rotor resistance, R_s is the stator resistance, σ is the leakage factor, L_s is the stator inductance,L_m is the mutual inductance, L_r is the rotor inductance, i_{rd} is the *d*-axis rotor current, v_{rd} is the *d*-axis rotor voltage, i_{rq} is the *q*-axis rotor current,v_{rq} is the *q*-axis rotor voltage, and ω_r is the rotor speed.

The DFIG stator's active and reactive powers can be carried out using the rotor currents and considering the assumption in (1) such as

$$\begin{cases} P_s = -\frac{3}{2}\frac{L_m}{L_s} V_s i_{rq} \\ Q_s = \frac{3}{2}\left(\frac{V_s \varphi_s}{L_s} - \frac{L_m}{L_s} V_s i_{rd}\right) \end{cases} \tag{3}$$

where, P_s is the active power and Q_s is the reactive power.

The stator reactive and active powers can be controlled and directly regulated by the *d*-axis and *q*-axis using the rotor currents as shown in (3).

2.2. Grid modeling

The grid is emulated by three-phase voltage source connected to the DC-AC converter, called the grid side converter, through the *RL* filter as shown in Fig. 1. Using *d-q* reference frame, the dynamics of the grid currents, modelled at the filter circuit, is carried out by [21,22,25].

$$\begin{cases} \frac{di_d}{dt} = -\frac{R}{L} i_d + \omega i_q - \frac{V_s}{L} + \frac{1}{L} v_d \\ \frac{di_q}{dt} = -\frac{R}{L} i_q - \omega i_d + \frac{1}{L} v_q \end{cases} \tag{4}$$

where, *R* is the filter resistance, ω is the grid angular frequency, *L* is the filter inductance, i_d is the *d*-axis grid current, i_q is the *q*-axis grid current,v_d is the *d*-axis converter voltage, v_q is the *q*-axis converter voltage and GSC control is based on the synchronized vector control scheme with the voltage alignment (v_d, $v_q = 0$). The active-reactive power, using the voltage alignment assumption at the grid side, is expressed by

$$\begin{cases} P_g = v_d i_d \\ Q_g = -v_d i_q \end{cases} \tag{5}$$

where, P_g is the active power and Q_g is the reactive power.

The grid power, expressed in (5), can be directly controlled using the grid currents. The DC-link is represented by the capacitor converters as illustrated in Fig. 1 at the back-to-back converter. Its voltage dynamics is governed by the expression [22,25]

$$\frac{dV_{dc}}{dt} = \frac{v_d}{CV_{dc}} i_d - \frac{1}{C} I_r \tag{6}$$

where, I_r is the rotor current. The DC-link voltage can be controlled by the *d*-axis grid current according to the dynamics (6). This control loop ensures a proper active power transmitted from the rotor to the grid by the AC converters.

3. Vector control scheme

The control is based on the vector control scheme for the GSC and RSC for the grid-linked DFIG energy system. At the GSC, cascaded control loops are used to regulate the grid currents and the DC-link voltage to provide an optimum power transfer under a specified power factor. The outer control loop provides the DC-link voltage regulation to follow up a reference voltage. The inner control loop provides the *d-q* axis grid current regulation. The *d*-axis current reference i_d^* is provided by the outer control loop (voltage controller) and the *q*-axis current reference i_q^* is carried from (5) depending on the required reactive power. For the DC-link voltage controller, a proportional-integral (PI) controller is used and a hysteresis controller is used for the grid current controller as depicted in Fig. 1.

For the DC-link voltage dynamics, the PI control law is expressed as

$$i_d^* = K_{p1} e_v + K_{i1} \int e_v d\tau \tag{7}$$

where, $e_v = V_{dc}^* - V_{dc}$ is the following up error for the DC-link voltage, K_{p1} and K_{i1} are the proportional and integral parameters, respectively.

At the RSC, the stator active-reactive power is controlled by the rotor currents as shown in (3). From the rotor current dynamics (4), the PI control laws are provided by

$$\begin{cases} v_{rd}^* = K_{p2} e_d + K_{i2} \int e_d d\tau - \left(\sigma L_r s \omega_s i_{rq} + \frac{R_s L_m}{\omega_s L_s} V_s\right) \\ v_{rq}^* = K_{p3} e_q + K_{i3} \int e_q d\tau + \left(\sigma L_r \omega_s i_{rd} + \frac{sL_m}{L_s} V_s\right) \end{cases} \tag{8}$$

where, $e_d = i_{rd}^* - i_{rd}$ is the tracking error for *d*-axis rotor current, $e_q = i_{rq}^* - i_{rq}$ is the *q*-axis rotor current's tracking error, $K_{p2,3}$ are the proportional control parameters, and $K_{i2,3}$ are the integral control parameters.

In this control system, the parameters (K_{p1}, K_{i1}, K_{p2}, K_{i2} ,K_{p3} , K_{i3}) will be optimized to achieve fast response time and no-overshoot. Water cycle optimization algorithm will be applied for parametric optimization of the three PI controllers.

4. Water cycle optimization

Water cycle optimization algorithm (WCA) is a technique inspired by the continuous movement of water known as water cycle [23]. The snows, or raindrops, on the mountains or hills flow down through branches to form a river or a stream. The rivers-streams content will continue the journey to be collected in the sea. In addition, the water is evaporated and moved to the atmosphere to form clouds that will condense, under cold conditions, to return to the earth as rain.

At the start of the WCA algorithm, an initial population, formed of raindrops within the search space, is created to solve the optimization problem [23,24]. The best raindrop is selected as a sea, which is the optimum solution.

The raindrop, for a single solution, is a vector such as

$$\text{Raindrops} = [x_1, x_2, x_3, \cdots, x_N] \tag{9}$$

where, N is the dimension of the optimization problem, which represents the number of design variables.

For the optimal control design, the Raindrop vector includes the six parameters of the three PI controllers. Therefore, $N = 6$ and the vector, in (9), is given by

$$[x_1, x_2, x_3, x_4, x_5, x_6] = [K_{p1}, K_{i1}, K_{p2}, K_{i2}, K_{p3}, K_{i3}] \tag{10}$$

The parameters x_i $(i = 1 \cdots 6)$, of the Raindrop vector (9), are within the bound constraints such as

$$l_b \le x_i \le u_b \tag{11}$$

where, l_b is the lower bound and u_b is the upper bound.

The optimization algorithm starts by generating a population of raindrops, represented by the following matrix of size $(N_p \times N)$

$$\text{Population} = \begin{bmatrix} \text{Raindrops}_1 \\ \text{Raindrops}_2 \\ \vdots \\ \text{Raindrops}_{N_p} \end{bmatrix}$$

$$\begin{bmatrix} X^1 \\ X^2 \\ \vdots \\ X^{N_p} \end{bmatrix} = \begin{bmatrix} x_1^1 & \cdots & x_N^1 \\ \vdots & \ddots & \vdots \\ x_1^{N_p} & \cdots & x_N^{N_p} \end{bmatrix} \tag{12}$$

where, N_p is the population size, X^i is the position of Raindrops$_i$ and $i = 1, \cdots, N_p$.

The raindrops position is randomly generated by the expression

$$X^i = l_b + (u_b - l_b) \times \text{rand}(1, N) \tag{13}$$

The raindrops cost,C_i, is carried out using the following cost function

$$C_i = F(X^i) \tag{14}$$

where, F is the objective function and $i = 1, \cdots, N_p$.

In this work, the objective of the optimal control is minimizing the tracking errors (e_v, e_d, e_q) for the voltage control (7) and the current control (8). w_v, w_d and w_q are the weighting factors, respectively. Integral time square error (ITSE) performance criterion is selected as the objective function such as

$$F(X) = [\, w_v \quad w_d \quad w_q \,] \begin{bmatrix} \int_0^T t e_v^2 dt \\ \int_0^T t e_d^2 dt \\ \int_0^T t e_q^2 dt \end{bmatrix} \tag{15}$$

In order to carry out the objective function in (15), the DFIG energy system shown in Fig. 1 is simulated and run with the values of the raindrops position $X^i = [x_1^i, x_2^i, \cdots, x_N^i]$ assigned to the PI control parameters, in (7) and (8), such as

$$[K_{p1}, K_{i1}, K_{p2}, K_{i2}, K_{p3}, K_{i3}] = [x_1^i, x_2^i, x_3^i, x_4^i, x_5^i, x_6^i] \tag{16}$$

The costs, C_i in (14), are sorted in ascending order. The number, N_{sr}, of the best raindrops, with lower cost values, are assigned to a number of rivers (N_r) and one sea such as

$$N_{sr} = N_r + \underbrace{1}_{\text{sea}} \tag{17}$$

where, the sea is the raindrops with the smallest cost value among the minimum cost values.

In the optimization problem, the sea position is the optimal solution. The remaining population, N_{st}, includes the streams that have the possibility to flow to the rivers or directly to the sea. It is carried out by

$$N_{st} = N_p - N_{sr} \tag{18}$$

The streams are allocated to the rivers or the sea based on the flow intensity of the raindrop provided by [17,18]

$$NS_n = \text{round}\left\{ \left| \frac{C_n}{\sum_{i=1}^{N_{sr}} C_i} \right| \times N_{st} \right\}, n = 1, 2, \cdots, N_{sr} \tag{19}$$

where, NS_n is the number of streams flowing into certain rivers and sea.

The streams are moving towards the rivers and the rivers are moving towards the sea. The updated positions, for the streams and the rivers, are given by

$$\begin{cases} X_{\text{stream}}^{i+1} = X_{\text{stream}}^i + rand \times C \times \left(X_{\text{river}}^i - X_{\text{stream}}^i \right) \\ X_{\text{river}}^{i+1} = X_{\text{river}}^i + rand \times C \times \left(X_{\text{sea}}^i - X_{\text{river}}^i \right) \end{cases} \tag{20}$$

where, rand $\in [0 \quad 1]$ and C is a number greater than 1 (best value is 2).

The costs of the new positions are carried out using the procedure (14)–(16). If the stream cost is found to be less than the river cost, their positions will be exchanged. The same procedure occurs for the positions of the river and the sea. The river position, with the lowest cost, becomes the sea position. To avoid a rapid convergence of the optimization algorithm, the evaporation process occurs for the sea water in order to leave space for the streams or rivers to flow to the sea. This process is based on the following condition

$$\text{if} \left| X_{\text{sea}}^i - X_{\text{river}}^i \right| < d_{max} \; \textit{Conduct raining process and evaporation End} \tag{21}$$

where, $i = 1, 2, \cdots, N_{sr} - 1$ and d_{max} is a small number $(\to 0)$.

Any distance between the river and the sea, smaller than d_{max} indicates that the river has reached the sea. Therefore, the evaporation can be conducted and after enough evaporation, the raining process can start as observed in nature. A small value for d_{max} promotes near-sea search intensity, while a large value reduces near-sea search. Therefore, the intensity of the search near the sea (optimal solution) can be controlled by d_{max}, which is updated in decrease as follows

$$d_{\text{max}}^{i+1} = d_{\text{max}}^i - \frac{d_{\text{max}}^i}{\text{max\_iter}} \tag{22}$$

where, max_iter is the maximum iteration number and $i = 1, 2, \cdots,$ max_iter.

The raining process consists of forming streams from new raindrops in different positions expressed by

$$X_{\text{stream}}^{\text{new}} = l_b + (u_b - l_b) \times \text{rand}(1, N) \tag{23}$$

The optimization algorithm will continue the search process from (20) until reaching the stopping condition (max_iter). Finally, the sea position is the optimal solution and its values will be used for the PI control parameters (10) to minimize cost functions focused on the following up errors (e_v, e_d, e_q) either the d-q axes rotor current of DC-link voltage control. The flowchart illustrating the application of the water cycle optimization algorithm is given in Fig. 2.

5. Experimental results and discussion

The experimental setup of the DFIG energy system, depicted in Fig. 3, is used to assess the optimization design. System parameters are shown in Table 1. A four-quadrant dynamometer is the prime mover. The real-time control is processed by the OPAL-RT OP5600. Voltage and current measurements are handled by the

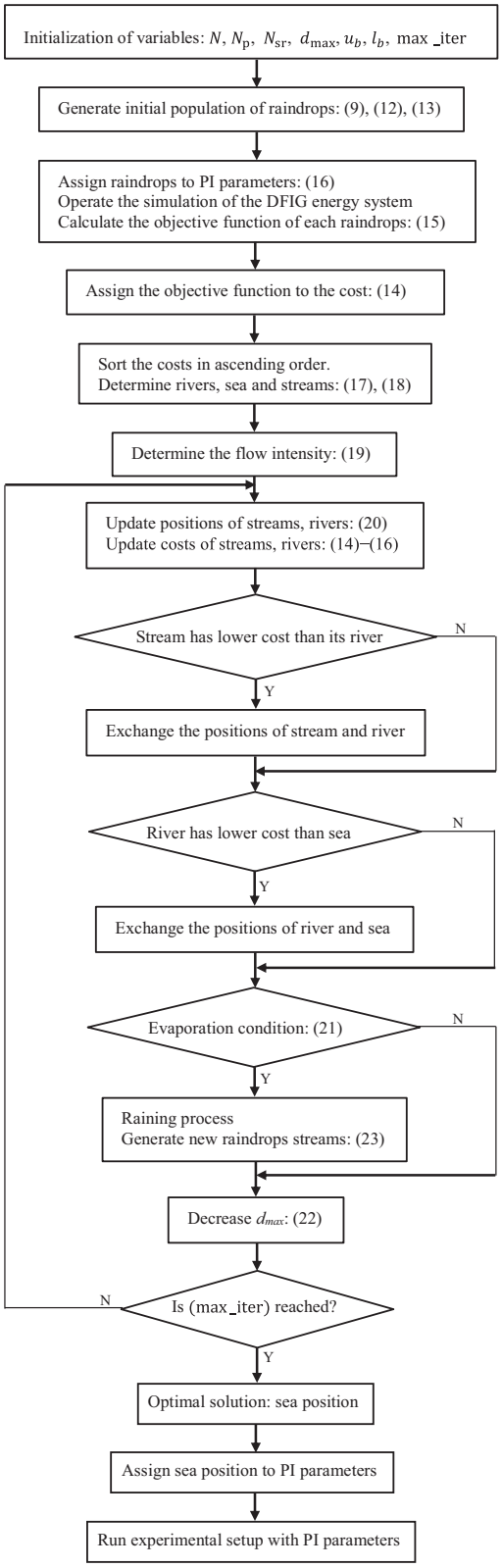

Fig. 2. Flowchart of the WCA algorithm.

data acquisition interface OPAL-RT OP8660. MATLAB/Simulink and RT-Lab software environment are used to build the real-time control system and hardware-in-the-loop. The DFIG energy system illustrated in Fig. 1 is simulated and controlled. Conventional,

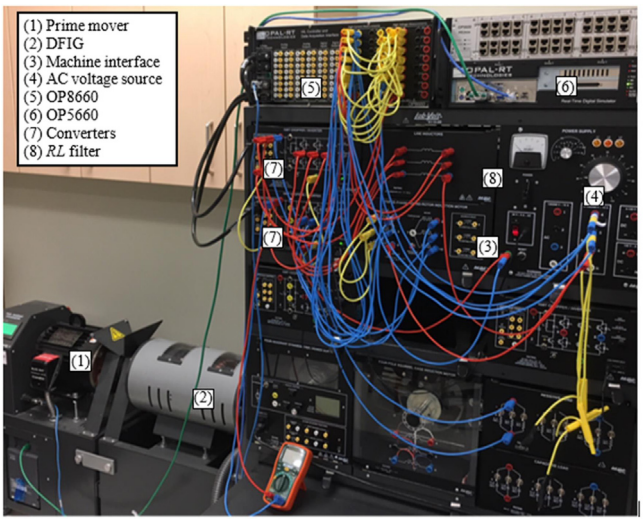

Fig. 3. DFIG energy system experimental setup.

Table 1
Doubly-fed induction generator parameters.

Parameters	Symbol	Quantity
Power	P_s	2 kW
Rotor voltage	V_r	120 V
Stator voltage	V_s	360 V
Stator current	i_s	10 A
Rotor current	i_r	3.3 A
Pole pairs	p	2
Nominal speed	w_{nom}	1700 rpm
Rotor inductance	L_r	0.0662 H
Stator inductance	L_s	0.0662 H
Mutual inductance	L_m	0.0945 H

GAO and WCA methods are carried out to optimize PI control parameters for d-q axes rotor current and DC-link voltage control, on the simulated DFIG energy system. The GAO and WCA optimization techniques were conducted using the performance criteria: integral time square error (ITSE), integral square error (ISE), integral time absolute error (ITAE), integral absolute error (IAE). Experimental results are collected to prove the effectiveness of the WCA method employing the optimized control parameters in the experimental DFIG setup, and its advantages over the conventional tuning design and the GAO method for parametric tuning of the PI controllers are demonstrated.

The conventional design method is based on a second-order system response by selecting the settling time (t_s) and the damping coefficient (ε) to evaluate the natural frequency (ω_n) and the parameters (K_p, K_i) of the PI controller [25,26].

The GAO technique is detailed in [27]. It is carried out using the parameters:

Population size: 50
Number of variables: 6
Rate of cross over: 0.8
Rate of mutation: 0.01
Number of iterations (Generations): 10, 100

The WCA technique is carried out using the parameters:

Number of variables (N): 6
Number of population (N_p): 50
Number of rivers + sea (N_{sr}): 4
Evaporation condition constant (d_{max}): 10^{-16}
Number of iterations (max_iter): 10, 100

The GAO and WCA methods were performed using the performance criteria ITAE, IAE, ITSE and ISE and the number of iterations equal to 10. The optimization was conducted off-line on a computer with the processor Intel(R) CPU@1.70 GHz Core(TM) i5-3317U. The optimization results are provided in Table 2. It can be noticed that the performance of WCA is superior to that of the GAO in terms of the mean error. Also, it is superior in terms of all performance criteria. However, the WCA method requires more execution time to achieve that performance.

For testing the experimental setup performance, the GAO and WCA methods were performed using the performance criterion ITSE and the number of generations and iterations are equal to 100. The DFIG energy system model was operated at a constant speed of 1650 rpm and used in the optimization method. The optimized values, for the PI control parameters were deployed in the vector control system shown in Fig. 1. The same values were used for all experiments. The goal of the optimization is to minimize response time, overshoot, and settling time in the tracking response.

Table 2
Statistical results of optimization.

Performance criterion	Control gain parameters	Genetic algorithm technique optimization	Water Cycle technique optimization
ITAE	DC-link voltage controller (K_{p1}, K_{i1})	0.901810, 0.084212	0.824910, 1
	d-axis current controller (K_{p2}, K_{i2})	0.917121, 0.670713	0.631795,
	q-axis current controller (K_{p3}, K_{i3})	0.926244, 0.487437	0.813323
	Best	0.06980	0.789344,
	Mean	0.08640	0.324237
	Elapsed time (sec)	13812.12	0.063385
			0.064210
			16987.4339
ITSE	DC-link voltage controller (K_{p1}, K_{i1})	0.905712, 0.934021	0.655728,
	d-axis current controller (K_{p2}, K_{i2})	0.950231, 0.636311	0.849184
	q-axis current controller (K_{p3}, K_{i3})	0.959714, 0.95931	0.822872,
	Best	1.5660	0.146304
	Mean	1.87196	0.959712,
	Elapsed time (sec)	12950.32	0.459390
			1.406088
			1.4791
			16730.1059
IAE	DC-link voltage controller (K_{p1}, K_{i1})	0.681474, 0.131560	0.792706,
	d-axis current controller (K_{p2}, K_{i2})	0.669862, 0.439013	0.029003
	q-axis current controller (K_{p3}, K_{i3})	0.754817, 0.156626	0.592603,
	Best	3.407847	0.499241
	Mean	3.66189	0.787434,
	Elapsed time (sec)	131221.43	0.000874
			3.30265
			3.32941
			16936.8080
ISE	DC-link voltage controller (K_{p1}, K_{i1})	0.665711, 0.859105	0.603819,
	d-axis current controller (K_{p2}, K_{i2})	0.823506, 0.157321	0.791254
	q-axis current controller (K_{p3}, K_{i3})	0.948731, 0.478309	0.517939,
	Best	342.7157	0.408270
	Mean	354.531	0.998447,
	Elapsed time (sec)	142311.35	0.006517
			340.24297
			342.568
			17615.40295

The DFIG system was operated under a fixed rotor speed (1650 rpm) in the first experiment. The voltage reference follows up-down step variations, at time instants t = 50 s and t = 60 s, from 295 V to 305 V and vice versa. Similar behavior was done for the references of the rotor *d-q* axes current. While getting real-time results, the time interval of 50–60 s is used for the DC-link response, while the time interval of 40–50 s is used for the d and q rotor current responses. The purpose of the study is to assign the control performance for each optimization method at the transitions. The control objective is tracking the specified references for the rotor *d-q* axes current and the DC-link voltage. In Fig. 4, the tracking responses are illustrated. As shown in Fig. 4.a, the voltage responses of GAO based PI control and the conventional one are underdamped with an overshoot while the response of the WCA PI controller is overdamped with better settling time. The WCA based response according to other comparison methods is efficient with regards to the settling time for the rotor d-q axes current, as shown in Fig. 4.b. and c.

Fig. 5 illustrates the WCA based optimal control performance for different number of iterations (*max_iter*) under the rotor d-q axes current and the DC-link voltage. It can be noticed that in Fig. 5.a, at a low number, the voltage response is underdamped and increasing the number to 50 and 100 makes it overdamped with improved settling time. In the rotor currents, illustrated in Fig. 5. b and c, the settling time is reduced with increasing iteration numbers.

In this experiment, the optimized PI parameters were deployed to operate the experimental DFIG energy system under variable rotor speed. The DFIG system was run under variable rotor speed (1650 rpm in [0 20]s, 1700 in [20 40]s, 1750 in [40 60]s, 1700 in [60 80]s and 1650 in [80 90]s). The components of the rotor current are the most influenced by the variations of the rotor speed from the DFIG dynamics (2), (4) and (6). The results are illustrated in Fig. 6. It can be detected that the DC-link voltage regulation is affected by speed variations in case of the conventional method, whereas the WCA and GAO provide good performance as shown in Fig. 6.a. Concerning the rotor *d-q* axes current responses, shown in Fig. 6.b and c, the WCA optimized PI controllers compared to GAO and conventional controllers react better to the rotor speed variations with respect to settling time and overshoot. Furthermore, the settling time at the transient regime, for the controlled variables *d-q* axes rotor current and DC-link voltage, is better for the WCA in comparison to the GAO and conventional methods as shown in Fig. 7.

Finally, the transient regime response of the voltage is compared using WCA method, for performance criteria IAE, ITAE, ISE, and ITSE. According to the results depicted in Fig. 8, the best settling time belongs to the ITSE performance criterion and the best overshoot belongs to the ISE criterion. It can be seen from the results in Table 2 that the WCA method gives better results for ITSE criterion. It is worth mentioning that the responses in Figs. 7 and 8 were delayed in order to separately visualize the settling time. These results were obtained to demonstrate the effect of different performance criteria on the results, which is another important aspect of the study that makes it possible to experimentally evaluate the proposed system according to various performance criteria.

In Fig. 9, fitness function comparison for performance criteria for ITSE and ISE is given. In Fig. 10, active and reactive powers are controlled by changing and controlling the rotor q current, and power profiles for stator, rotor and network are given. From the power responses shown in Fig. 10, it can be observed that

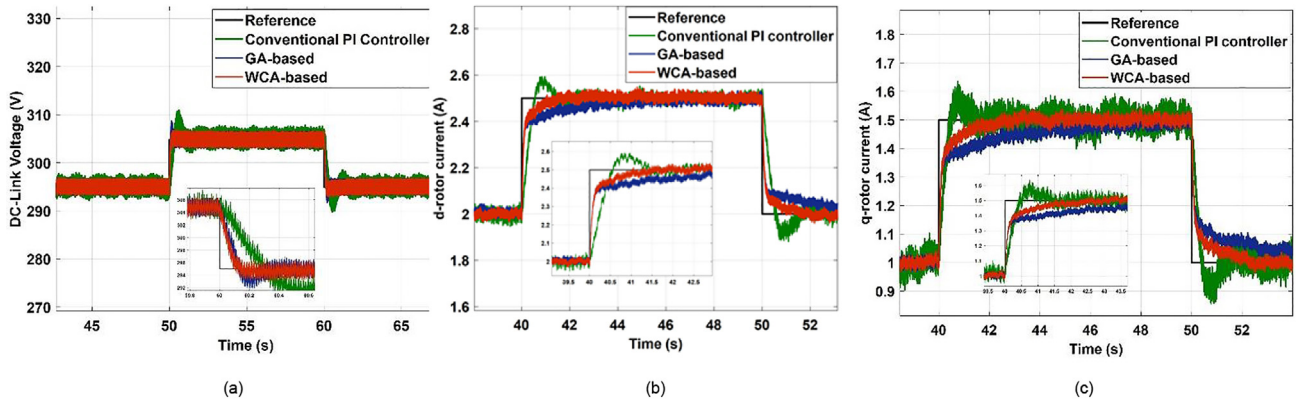

Fig. 4. (a) DC-link voltage (b) d-axis current (c) q-axis current (Tracking responses of the optimization techniques under constant rotor speed).

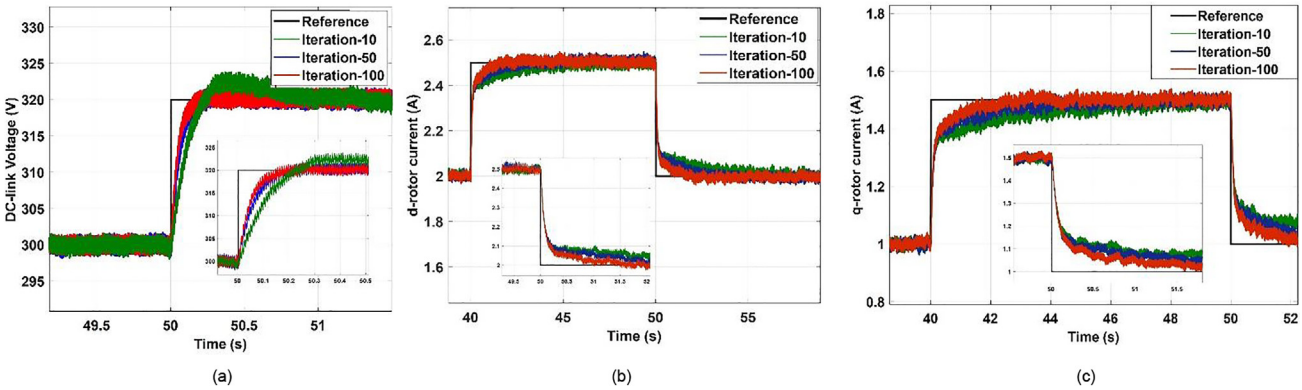

Fig. 5. (*a*) DC-link voltage (*b*) *d*-axis current (*c*) *q*-axis current (Tracking responses of WCA under different number of iterations).

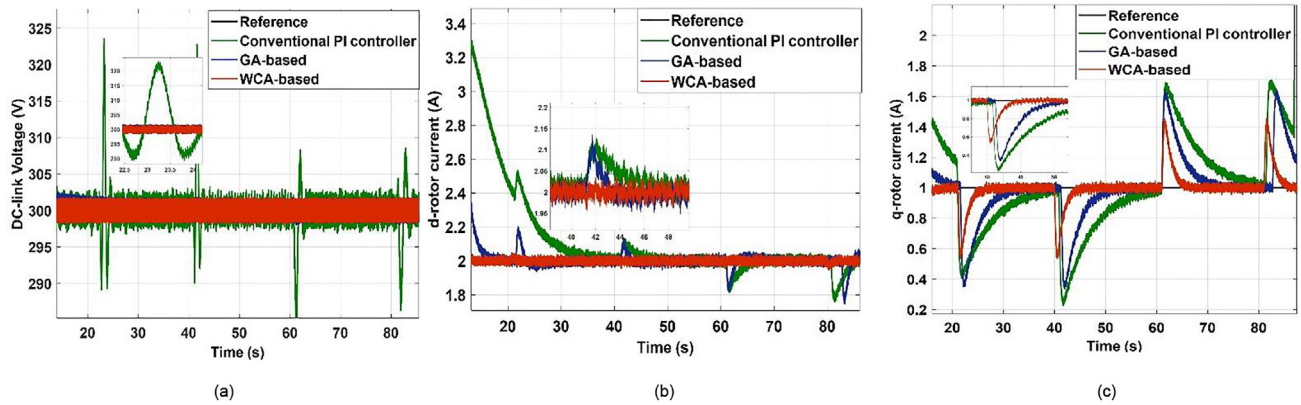

Fig. 6. (*a*) DC-link voltage (*b*) *d*-axis current (*c*) *q-axis* current (Tracking responses of the optimization techniques under variable rotor speed).

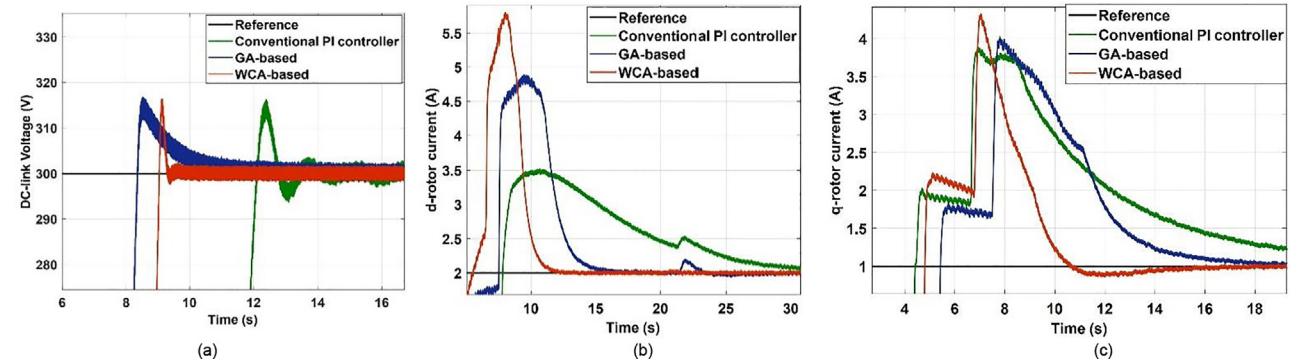

Fig. 7. (a) DC-link voltage (b) *d*-axis current (c) *q*-axis current (Transient responses of the optimization techniques under variable rotor speed).

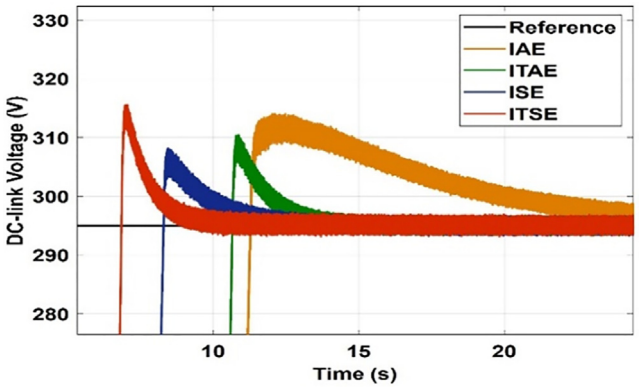

Fig. 8. Transient responses of the WCA under different performance criteria.

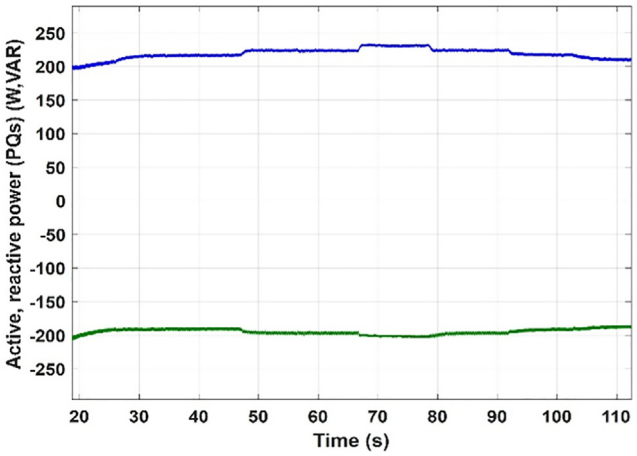

Fig. 10. Active and Reactive power responses.

the active and reactive powers can be controlled by changing the rotor current. In Fig. 10, active power shown in blue increases to balance the total while reactive power shown in green decreases.

Likewise, when the I_d current is changed in the system, the active power decreases to balance the total while the reactive power increases. Active and reactive powers and changes in the system are observed in this wind energy system by keeping the dc link voltage V_{dc} constant and changing the i_d and i_q currents. The effect of the change of i_d and i_q on the system and the changes in the power profile can be seen. In addition, the DC-link voltage has been successfully arranged to follow a continuous reference. The dynamic time responses, for the step transition at 50 s in Fig. 4, are presented in Table 3, where the superiority of the WCA compared to GA and conventional methods can be observed with respect of overshoot and settling time. As can be seen in Table 3, the overshoot for the dc link controller decreased from 52.12% to 11.08%, the settling time fell from 1.340 to 0.67.

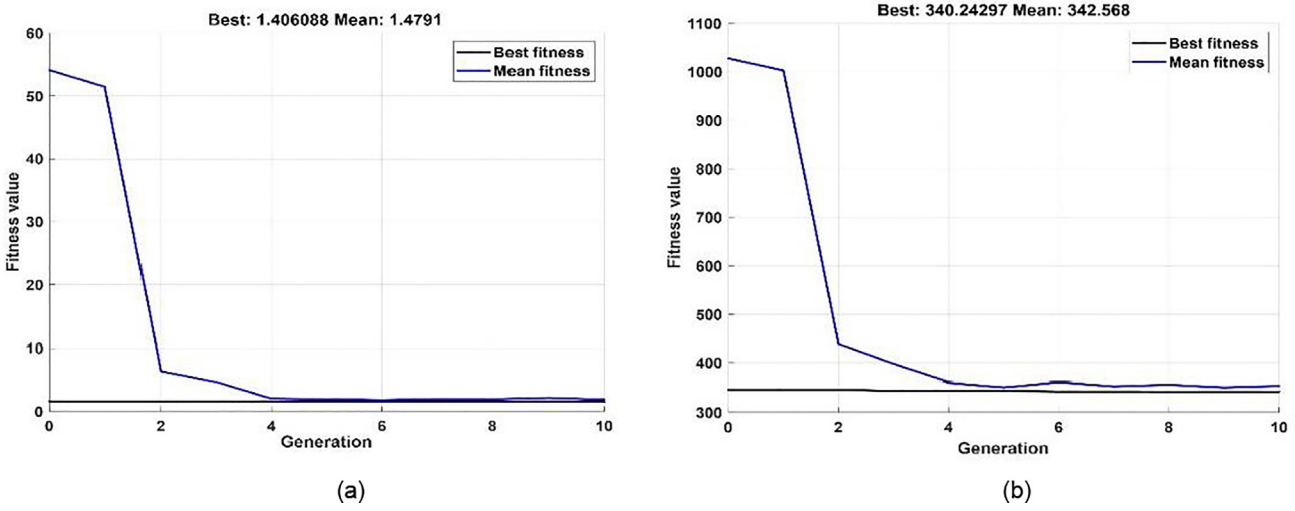

Fig. 9. Fitness function comparison for performance criteria in terms of (a) ITSE, (b) ISE.

Table 3
Dynamic performance for experimental results.

Controller	Methods Overshoot (%)	Settling time (s)	Peak Values
DC-link voltage (V)	*Conventional* 52.12	1.340	310.2
	GA 26.92	0.8	307.9
	WCA 11.08	0.67	306.0
d-rotor current (A)	*Conventional* 8.90	2.5	2.58
q-rotor current (A)	*GA* 3.202	1.5	2.503
	WCA 1.27	1.04	2.501
	Conventional 9.08	2.1	1.609
	GA 2.06	1.09	1.52
	WCA 1.01	0.9	1.51

6. Conclusions

The parameters of the PI controllers, in a grid-linked DFIG energy system, were optimized using a nature-inspired computing tool based on the water cycle. The vector control scheme of the energy system includes three PI controllers for the rotor d-q axis current and the DC-link voltage. The water cycle optimization technique was implemented to minimize a cost function carried out from the tracking errors to optimize the control parameters. Different performance criteria were investigated for comparison purposes. Experimentation was carried out on an experimental DFIG energy system, using control parameters optimized by conventional, genetic algorithms and water cycle methods, under fixed and variable rotor speed. It was found that the water cycle optimization provides superior performance according to the overshoot and the response time. From the dynamic time responses given in Table 3, obtained for the step transition at 50 s in Fig. 4, the peak value of the conventional method is 310.2 V while the peak value of the WCA-based method is 306 V, according to a reference value of 305 V. As a result, in the WCA based method the voltage fluctuation was reduced by 1.35% compared to the conventional method. Furthermore, it was found that the ITSE based cost function provides better tracking response. Although the water cycle optimization requires more execution time, this does not pose any drawback as these computations are done off-line. Besides, different from the classical PI tuning methods, the trial and error based methods are not used in tuning and therefore the design time can be further reduced without altering the optimization quality. Finally, it can be concluded that the water cycle optimization is a practical tool in optimal control for physical applications.

Declaration of Competing Interest

The authors declare that they have no known competing financial interests or personal relationships that could have appeared to influence the work reported in this paper.

Acknowledgments

The Canada Innovation Foundation for Grant 30527 and the Scientific and Technological Research Council of Turkey (TUBITAK) under Grant BIDEB-2214 have supported this work.

References

[1] S. Chatterjee, A. Naithani, V. Mukherjee, Small-signal stability analysis of DFIG based wind power system using teaching learning based optimization, Int. J. Electr. Power Energy Syst. 78 (2016) 672–689.
[2] H. Bakir, A.A. Kulaksiz, Modelling and voltage control of the solar-wind hybrid micro-grid with optimized STATCOM using GA and BFA, Eng. Sci. Technol. Int. J. 23 (3) (2020) 576–584.
[3] M. M. Alhato, S. Bouallègue, Direct power control optimization for doubly fed induction generator based wind turbine systems, Math. Comput. Appl., vol. 24, no. 77, 2019.
[4] R. C. Bansal, T. S. Bhatti, V. Kumar, Reactive power control of autonomous wind-diesel hybrid power systems using ANN, in Proc. Int. Power Engineering Conf., Singapore, Singapore, Dec. 3–6, 2007.
[5] M. Li, P. Zhou, Z. Zhao, J. Zhang, Two-degree-of-freedom fractional order-PID controllers design for fractional order processes with dead-time, ISA T. 61 (2016) 147–154.
[6] S. Banerjee, T.K.S. Kumar, J. Pal, D. Prasad, Controller design for large-gap control of electromagnetically levitated system by using an optimization technique, IEEE Trans. Control Syst. Technol. 16 (3) (2008) 408–415.
[7] C.H. Hsieh, J.H. Chou, Design of optimal PID controllers for PWM feedback systems with bilinear plants, IEEE Trans. Control Syst. Technol. 15 (6) (2007) 1075–1079.
[8] H. Bevrani, F. Habibi, P. Babahajyani, M. Watanabe, Y. Mitani, Intelligent frequency control in an AC Microgrid: online PSO-based fuzzy tuning approach, IEEE Trans. Smart Grid 3 (4) (2012) 1935–1944.
[9] H.M. Hasanien, S.M. Muyeen, Design optimization of controller parameters used in variable speed wind energy conversion system by genetic algorithms, IEEE Trans. Sustain. Energy 3 (2) (2012) 200–208.
[10] M.N. Ambia, H.M. Hasanien, A. Al-Durra, S.M. Muyeen, Harmony search algorithm based controller parameters optimization for a distributed generation system, IEEE Trans. Power Del. 30 (1) (2015) 246–255.
[11] H. Keshta, A. Ali, E. Saied, F. Bendary, Comparative performance of wind energy conversion system (WECS) with PI controller using heuristic optimization algorithms, CIRED - Open Access Proc. J. 2017 (1) (2017) 549–553.
[12] J.W. Perng, Y.C. Kuo, K.C. Lu, Design of the PID controller for hydro-turbines based on optimization algorithms, Int. J. Control Autom. Syst. 18 (2020) 1758–1770.
[13] M. E. Colak, A. Varol, A Novel Intelligent Optimization Algorithm Inspired from Circular Water Waves, Elektronika Ir Elektrotechnika, vol. 21 no.5, p.p 3-6, 2015.
[14] S. Yilmaz, E.U. Kucuksille, Y. Cengiz, Modified bat algorithm, Elekronika Ir Elektrotechnika 20 (2) (2014) 71–78.
[15] R. Kumara, R. Singha, H. Ashfaqa, S. K. Singh, M. Badonic, Power system stability enhancement by damping and control of Sub-synchronous torsional oscillations using Whale optimization algorithm based Type-2 wind turbines, ISA Transactions, In press, corrected proof, 2020.
[16] X. Yang, J. Long, P. Liu, Xi. Zhang, Xi. Liu, Optimal scheduling of microgrid with distributed power based on water cycle algorithm, Energies, vol. 11, pp. 2381, 2018.
[17] M.A. Elhameed, A.A. El-Fergany, Water cycle algorithm-based load frequency controller for interconnected power systems comprising non-linearity, IET Gener. Transm. Dis. 10 (15) (2016) 11–17.
[18] H.M. Hasanien, M. Matar, Water cycle algorithm-based optimal control strategy for efficient operation of an autonomous microgrid, IET Gener. Transm. Dis. 12 (21) (2018) 5739–5746.
[19] M.M. Alhato, S. Bouallegue, M. Ayadi, Water cycle algorithm-tuned PI control of a doubly fed induction generator for wind energy conversion, 9th International Renewable Energy Congress (IREC) (2018).
[20] S.A.M. Abdelwahab, A.M. Yousef, M. Ebeed, F.K. Abo-Elyousr, A. Elnozohy, M. Mohamed, Optimization of PID controller for hybrid renewable energy system using adaptive sine cosine algorithm, Int. J. Renew. Energy Res.-IJRER 10 (2) (2020) 670–677.
[21] A. Merabet, H. Eshaft, A. Tanvir, Power-current controller based sliding mode control for DFIG-wind energy conversion system, IET Renew. Power Gen. 12 (10) (2018) 1155–1163.
[22] A. Tanvir, A. Merabet, R. Beguenane, Real-time control of active and reactive power for doubly fed induction generator (DFIG)-based wind energy conversion system, Energies 8 (2015) 10389–10408.
[23] H. Eskandar, A. Sadollah, A. Bahreininejad, M. Hamdi, Water cycle algorithm – a novel metaheuristic optimization method for solving constrained engineering optimization problems, Comput. Struct. 110–111 (2012) 151–166.
[24] A. Sadollaha, H. Eskandar, H.M. Lee, D.G. Yoo, J.H. Kim, Water cycle algorithm: a detailed standard code, Software X 5 (2016) 37–43.
[25] R. Teodorescu, M. Liserre, P. Rodriguez, Grid converters for photovoltaic and wind power systems, Publication, John Wiley & Sons Ltd, 2011.
[26] H. Bakir, A. Merabet, R.K. Dhar, A.A. Kulaksiz, Bacteria foraging optimisation algorithm based optimal control for doubly-fed induction generator wind energy system, IET Renew. Power Gener. 14 (11) (2020) 1850–1859.
[27] L.H. Hassan, M.M. Haider, A.F. Almurib, K.M. Muttaqi, V.G. Ganapathy, Optimization of power system stabilizers using participation factor and genetic algorithm, Int. J. Elec. Power 55 (2014) 668–679.